



Glycolate production by a *Chlamydomonas reinhardtii* mutant lacking carbon-concentrating mechanism

Eun Ju Yun^{a,b,1}, Guo-Chang Zhang^{b,1}, Christine Atkinson^{b,d,1}, Stephan Lane^{b,d}, Jing-Jing Liu^b, Donald R. Ort^{b,c}, Yong-Su Jin^{b,d,*}

^a Department of Biotechnology, Graduate School, Korea University, Seoul, 02841, Republic of Korea

^b Carl R. Woese Institute for Genomic Biology, University of Illinois at Urbana-Champaign, Urbana, IL, 61801, USA

^c Department of Plant Biology, University of Illinois at Urbana-Champaign, Urbana, IL, USA

^d Department of Food Science and Human Nutrition, University of Illinois at Urbana-Champaign, Urbana, IL, USA

ARTICLE INFO

Keywords:

Chlamydomonas reinhardtii

Glycolate

CIA5

Photorespiration

Carbon-concentrating mechanism (CCM)

ABSTRACT

The green alga *Chlamydomonas reinhardtii* serves as a model organism for plant and photosynthesis research due to many commonalities in metabolism and to the fast growth rate of *C. reinhardtii* which accelerates experimental turnaround time. In addition, *C. reinhardtii* is a focus of research efforts in metabolic engineering and synthetic biology for the potential production of biofuels and value-added chemicals. Here, we report that the *C. reinhardtii* *cia5* mutant, which lacks a functional carbon-concentrating mechanism (CCM), can produce substantial amounts of glycolate, a high-value cosmetic ingredient, when the mutant is cultured under ambient air conditions. In order to reveal the metabolic basis of glycolate accumulation by the *cia5* mutant, we investigated the metabolomes of the *cia5* mutant and a wild type strain CC-125 (WT) through the global metabolic profiling of intracellular and extracellular fractions using gas chromatography and mass spectrometry. We observed the intracellular and extracellular metabolic profiles of the WT and the *cia5* mutant were similar during the mixotrophic phase at 30 h. However, when the cells entered the photoautotrophic phase (i.e., 96 h and 120 h), both the intracellular and extracellular metabolic profiles of *cia5* mutant differed significantly when compared to WT. In the *cia5* mutant strain, a group of photorespiration pathway intermediates including glycolate, glyoxylate, glycine, and serine accumulated to significantly higher levels compared to WT. In the photorespiration pathway, glycolate is metabolized to glyoxylate and glycine leading to NH₃ and CO₂ generation during the mitochondrial conversion of glycine to serine. This result provides further evidence that the *CIA5* mutation increased the photorespiration rate. Because the *cia5* mutant lacks a CCM, and *C. reinhardtii* might harbor an inefficient or incomplete photorespiration pathway, glycolate may accumulate when the CCM is not functional. We envision that investigating photorespiration controls in *C. reinhardtii* provides tools for producers to use the *cia5* mutant to produce glycolate as well as platform to engineer alternative pathways for glycolate metabolism.

1. Introduction

In photosynthesis, ribulose 1,5-bisphosphate carboxylase/oxygenase (Rubisco) catalyzes the fixation of inorganic carbon (i.e., CO₂) to ribulose 1,5-bisphosphate (RuBP) and generates two molecules of 3-phosphoglycerate (Fig. 1A). Alternatively, its oxygenase mode, Rubisco fixes O₂ from the atmosphere to RuBP and generates one 3-carbon unit (i.e., 3-phosphoglycerate) and one 2-carbon unit (i.e., 2-phosphoglycolate) (Fig. 1A). While 3-phosphoglycerate can re-enter the

photosynthetic cycle, 2-phosphoglycolate cannot and in addition 2-phosphoglycolate inhibits the activity of enzymes involved in the Calvin-Benson cycle (e.g., Deller et al., 2016). Photosynthetic eukaryotes have evolved a complicated and energy-consuming photorespiration pathway to detoxify and recycle glycolate to generate glycerate and evolve a CO₂ (Fig. 1B). The Rubisco functionality changes based on the nearby O₂ and CO₂ concentrations so that organisms that concentrate inorganic carbon near the site of Rubisco can increase the carboxylase rate at the expense of the oxygenase rate and thereby increase net

* Corresponding author at: Carl R. Woese Institute for Genomic Biology, University of Illinois at Urbana-Champaign, Urbana, IL, 61801, USA.

E-mail address: ysjin@illinois.edu (Y.-S. Jin).

¹ These authors contributed equally to this work

2. Materials and methods

2.1. Strains and culture conditions

We purchased *C. reinhardtii* CC-125 (WT) and CC-2702 (*cia5* mutant) strains from the Chlamydomonas Resource Center (<http://www.chlamycollection.org>) and cultivated the strains in 125-mL flasks of liquid Tris-Acetate-Phosphate (TAP) medium on a shaker platform set at 100 rpm (Gorman and Levine, 1965). Flasks were continuously illuminated at $65 \mu\text{mol m}^{-2} \text{s}^{-1}$ (Li-COR model Li-189, sensor = Quantum (Q40180)) using cool-white fluorescent light (GE Ecolux w/ Starcoat 4100 K 32 W) at 25 °C. The cultures were maintained using ambient air within the flask, and the flasks were covered with aluminum foil. There was no additional CO₂ provided. Cell growth was monitored by measuring the optical density at 750 nm (OD₇₅₀) using a Biomate 3S (Thermo Electron Corporation, Waltham, MA, US).

2.2. High-performance liquid chromatography

We monitored the acetate consumption and the glycolate production in the WT and *cia5* mutant strains using high-performance liquid chromatography (HPLC; Agilent Technologies, Waldbronn, Germany) equipped with a refractive index detector and an H + column (Rezex ROA-Organic Acid; Phenomenex, Torrance, CA). We set the column temperature and the refractive index detector to 50 °C. We used 2.5 mM H₂SO₄ as a mobile phase and set the flow rate to 0.6 mL/min.

2.3. Preparation of the samples for metabolic profiling by GC/MS

For intracellular metabolite analysis, we used the methanol quenching method as previously described with a slight modification (Kim et al., 2013). Briefly, we collected cells during culture and twice washed the cells using ice-cold water. We quickly mixed the washed cells with 1 mL of a pre-chilled acetonitrile–water mixture (1:1, v/v) and 100 μL of glass beads. Then, we vortexed the extraction mixture for 3 min to extract intracellular metabolites of WT and *cia5* mutant strains by disruption of the cell membrane and centrifuged the mixture at 16,100 $\times g$ for 3 min at 4 °C. We took 0.8 mL of the supernatant containing the intracellular metabolites and dried the material in a speed vacuum concentrator for 6 h.

To analyze extracellular metabolites, we dried 20 μL of the culture supernatant in the speed vacuum concentrator for 6 h. All experiments were performed in triplicate at three different sampling timepoints (i.e., 30 h, 96 h, and 120 h).

2.4. Metabolite profiling by GC/MS

Before GC/MS analysis, we derivatized the extracted metabolites by methoxyamination and trimethylsilylation (Lee and Fiehn, 2008). The methoxyamination step began as we added 10 μL of 40 mg/mL methoxyamine chloride in pyridine (Sigma-Aldrich, St. Louis, MO, US) to the samples and then incubated the samples for 90 min at 30 °C, shaking at 200 rpm. Then, we added 45 μL of *N*-methyl-*N*-trimethylsilyltrifluoroacetamide (MSTFA; Sigma-Aldrich) to the samples for trimethylsilylation and incubated for 30 min at 37 °C and 200 rpm shaking. For the detection of small molecular weight compounds such as glycolate, we performed *tert*-butyldimethylsilylation instead of trimethylsilylation by adding 45 μL of *N*-*tert*-butyldimethylsilyl-*N*-methyltrifluoroacetamide (MTBSTFA; Sigma-Aldrich) instead of MSTFA.

For GC/MS analysis, we applied the derivatized metabolite samples to an Agilent 7890A GC/5975C MSD system (Agilent Technologies, Wilmington, DE) equipped with an RTX-5Sil MS capillary column (30 m \times 0.25 mm, 0.25 μm film thickness; Restek, Bellefonte, PA) and an additional 10-m-long integrated guard column. We injected one microliter of the derivatized sample into the GC inlet in splitless mode.

Initially, the oven temperature was set to 150 °C for 1 min, after which the temperature increased to 330 °C at 20 °C/min, where it remained for 5 min after reaching 330 °C. The system recorded the mass spectra in a scan range 85–500 m/z at electron impact of 70 eV, and the temperatures of the ion source and transfer line were 230 °C and 280 °C, respectively (Lee and Fiehn, 2008).

2.5. Metabolite data processing and statistical analyses

We preprocessed the raw data obtained from GC/MS analysis in an automated mass spectral deconvolution and identification system (AMDIS) software (Stein, 1999) for peak detection and deconvolution. Then, we uploaded the pre-processed data into SpectConnect (Styczynski et al., 2007) for peak alignment and for generation of the data matrix with Golm Metabolome Database (GMD) mass spectral reference library. We obtained the normalized abundance values for each metabolite by dividing peak intensity with dry cell weight. For multivariate statistical analysis and clustering analysis, such as principal component analysis (PCA) and hierarchical cluster analysis (HCA), we used Statistica (version 7.1; StatSoft, Palo Alto, CA) and MultiExperiment Viewer software (Howe et al., 2010), respectively.

3. Results

3.1. Growth profiles of *C. reinhardtii* WT and *cia5* mutant

We monitored cell growth, acetate consumption, and extracellular metabolite production by *C. reinhardtii* CC-125 (WT) and CC-2702 (*cia5* mutant) strains (Fig. 2). We added acetate (1.0 g/L) into the culture broth as a carbon source for both WT and *cia5* mutant strains. Growth profiles for both strains as measured by OD₇₅₀ were similar during the acetate-consuming phase (i.e., mixotrophic phase) (Fig. 2A). Intriguingly, after acetate depletion at approximately 72 h and the start of the photoautotrophic phase, the *cia5* mutant started to produce glycolate, the key metabolic substrate for the photorespiration pathway (Fig. 2B). Meanwhile, WT did not produce glycolate at all during the photoautotrophic phase (Fig. 2B). During the photoautotrophic phase, the OD₇₅₀ values decreased in the *cia5* mutant, whereas those obtained from WT increased slightly (Fig. 2A).

3.2. Analysis of the intracellular and extracellular metabolites of WT and *cia5* mutant

We investigated the metabolic basis that led the *cia5* mutant to accumulate glycolate by using a principal component analysis (PCA) of WT and *cia5* mutant metabolites obtained from GC/MS analysis data (Fig. 3A and B). In total, 54 intracellular metabolites and 24 extracellular metabolites belonging to amino acids, sugars, organic acids, fatty acids, phosphates, and nucleosides were identified in WT and *cia5* mutant (Table S1 and S2). Interestingly, two dimensional PCA results obtained from intracellular metabolites of WT and *cia5* mutant showed a clear separation between the two different growth phases, a mixotrophic phase and a photoautotrophic phase, and the two different strains, WT and *cia5* mutant, with an R^2X value of 0.535, which indicates goodness of fit of the PCA model (Fig. 3A). More specifically, PC1 majorly contributed to discriminate two different growth phases (i.e., a mixotrophic phase and a photoautotrophic phase). Meanwhile, PC2 contributed to discriminate two different strains, WT and *cia5* mutant, during the photoautotrophic phase (Fig. 3A).

The PCA results of extracellular metabolites of WT and *cia5* mutant differed with those obtained from intracellular metabolites (Fig. 3A and B). Only the extracellular metabolite profiles obtained from *cia5* mutant during a photoautotrophic phase (i.e., CIA5_96 h and CIA5_120 h) were discriminated from the other conditions by PC1 (Fig. 3B). The metabolite profiles of *cia5* mutant during a mixotrophic phase (i.e., CIA5_30 h) or of WT during both a mixotrophic phase and a photoautotrophic phase

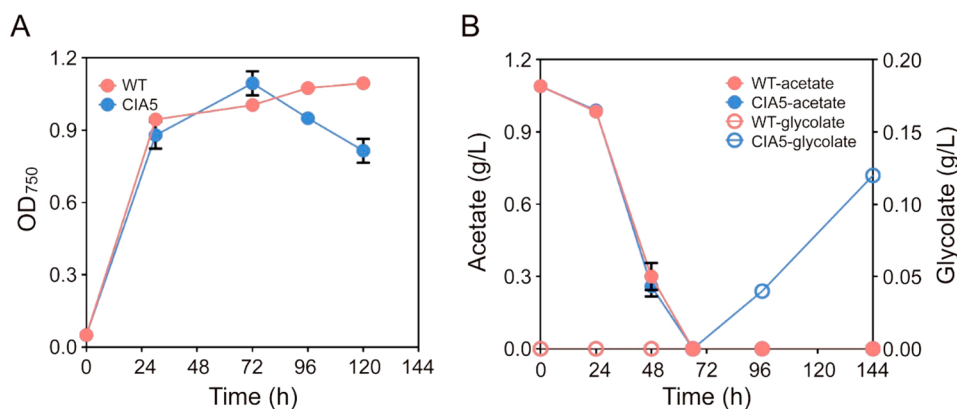


Fig. 2. Comparison of the cell growth, acetate consumption, and glycolate production profiles for *Chlamydomonas reinhardtii* WT (WT) and *cia5* mutant (CIA5) strains. (A) Cell growth and (B) acetate consumption and glycolate production of WT and CIA5.

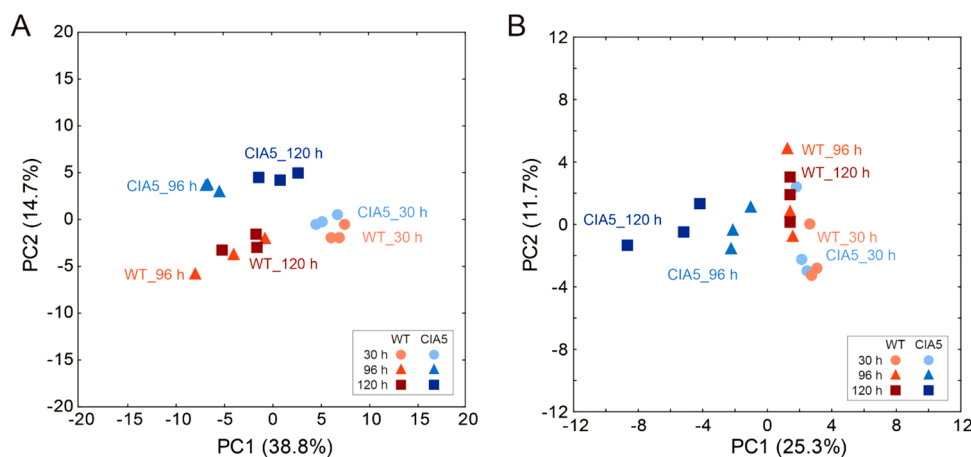


Fig. 3. The two-dimensional PCA scatter plots generated from (A) the 54 intracellular metabolites and (B) the 24 extracellular metabolites of *Chlamydomonas reinhardtii* WT (WT) and *cia5* mutant (CIA5) strains. The labels in the PCA scatter plot represent the two different strains (i.e., WT and CIA5) with three different sampling time points (i.e., 30 h, 96 h, and 120 h). All experiments were performed in triplicate.

(i.e., WT_30 h, WT_96 h, and WT_120 h) were not discriminated PCA analysis (Fig. 3B).

We listed the loading scores for the 54 intracellular and 24 extracellular metabolites on PC1 and PC2 in Table S3 and S4, respectively. Of the total metabolites identified in this study, we focused on the loading scores of the metabolites found in photorespiration, photosynthesis, and glycolysis pathways. In the intracellular PCA results, the metabolic intermediates of glycolysis such as 3-phosphoglycerate, pyruvate, and dihydroxyacetone phosphate made a positive contribution to PC1 (Fig. 3A and Table S3). Meanwhile, the metabolic intermediates involved in photorespiration pathway such as glycolate, glycine, and serine made a positive contribution to PC2 (Fig. 3A and Table S3). However, in the extracellular PCA results, the metabolic intermediates of photorespiration pathway such as glutamate, glycine, and glycolate made a negative contribution to PC1 (Fig. 3B and Table S4).

3.3. Clustering analysis of the metabolites obtained from *C. reinhardtii* CC-125 and *cia5* mutant

We selected 18 samples (two different strains × three different sampling time points × triplicates) from the identified intracellular and extracellular metabolites and subjected them to hierarchical clustering analysis (HCA) to identify possible differences in the intracellular and extracellular metabolite profiles of the WT and the *cia5* strain. Clustering of intracellular metabolites resulted in good separation based on the strains, WT and *cia5* mutant, and sampling time points (Fig. 4A).

More specifically, intracellular metabolites obtained from mixotrophic phase and photoautotrophic phase separated regardless of the strain background (Fig. 4A). During the mixotrophic phase, pyruvate, 3-phosphoglycerate, and dihydroxyacetone phosphate accumulated at high levels in both WT and *cia5* mutant (Fig. 4A). However, we noticed most of the identified intracellular metabolites accumulated during the photoautotrophic phase in both strains. After entering the photoautotrophic phase at 96 h and 120 h, the metabolite profiles were clustered based on the types of strains, WT and *cia5* mutant (Fig. 4A). Also, in *cia5* mutant at 120 h, the abundances of the metabolites such as glucose, glucose 6-phosphate, malate, and fumarate, which are involved in the central carbon metabolism were significantly reduced compared to the results obtained from *cia5* mutant at 96 h (Fig. 4A). This is probably due to the cell death of *cia5* mutant caused by the continued low net photosynthetic activity in the photoautotrophic phase.

Meanwhile, extracellular metabolites clusters separated *cia5* mutant during photoautotrophic phase from other phases (Fig. 4B). During the photoautotrophic phase, the amino acids closely related to photorespiration pathway (i.e., serine, glycine, and glutamate) and C2 compounds involved in the photorespiration pathway (i.e., glyoxylate and glycolate) were significantly accumulated in the *cia5* mutant culture (Fig. 4B).

3.4. Metabolomic changes related to photosynthesis

According to the PCA and HCA analyses described above, the metabolite profiles of the *C. reinhardtii* WT and the *cia5* mutant differed

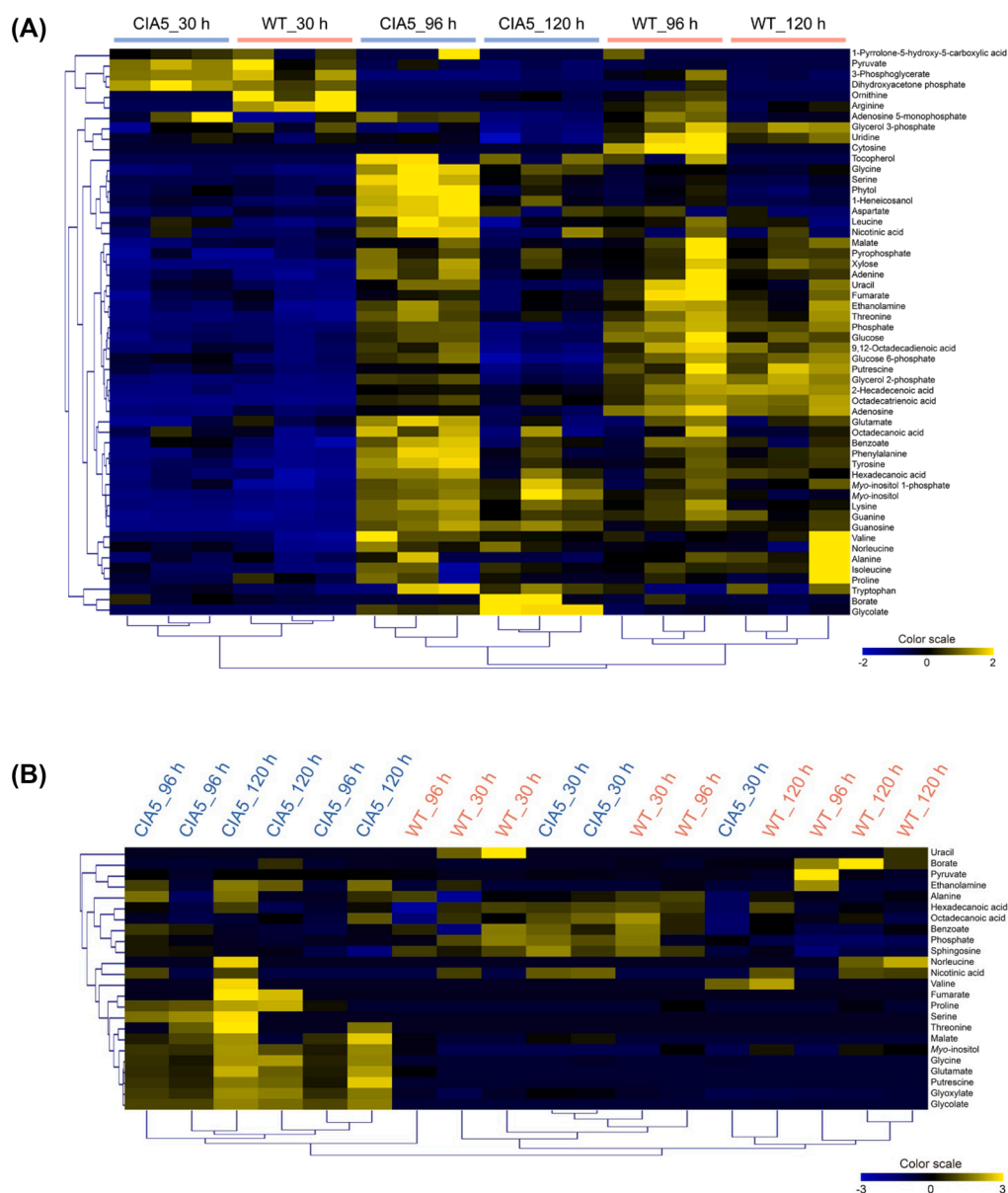


Fig. 4. The heat maps of (A) the 54 intracellular metabolites and (B) the 24 extracellular metabolites of *Chlamydomonas reinhardtii* WT (WT) and *cia5* mutant (CIA5) strains. The x-axis labels represent the two different strains (i.e., WT and CIA5) with three different sampling time points (i.e., 30 h, 96 h, and 120 h). The y-axis labels represent (A) the 54 intracellular metabolites and (C) the 24 extracellular metabolites identified in this study. All experiments were performed in triplicate.

significantly in the abundances of metabolic intermediates of photosynthesis and photorespiration pathways (Figs. 3 and 4). Among the metabolic intermediates of photosynthesis, 3-phosphoglycerate, generated via the reactions of RuBP and CO₂ by Rubisco, were greater in WT at 96 h as compared to the WT at 120 h and the *cia5* mutant at 96 h and 120 h (Fig. 5A). Glycerol 3-phosphate and glycerol 2-phosphate were abundant in WT at 96 h and 120 h as compared to *cia5* mutant at 96 h and 120 h (Fig. 5A). Glycerol phosphates, glycerol 3-phosphate and glycerol 2-phosphate, are metabolic intermediates of the glycerolipid pathway, which is a branched pathway derived from glycolysis (Riekhof et al., 2005). Furthermore, the intensities of glucose and glucose 6-phosphate, the intermediates of upper glycolysis, were elevated in WT at 96 h and 120 h and *cia5* at 120 h (Fig. 5A).

3.5. Metabolomic changes related to photorespiration

With regard to the photorespiration pathway, the *cia5* mutant accumulated significant amounts of glycolate both intracellularly and

extracellularly (Fig. 5B and C). Crucial amino acids involved in the photorespiration pathway — serine, glutamate, and glycine — increased in the *cia5* mutant at 96 h and 120 h (Fig. 5B). Among those, we also observed extracellular accumulation of glutamate and glycine (Fig. 5C). Most notably, the C2 compound glyoxylate, which is generated from glycolate, accumulated extracellularly in *cia5* mutant cultures at 96 h and 120 h (Fig. 5C).

3.6. Production of glycolate by *cia5* mutant strain

Based on the results obtained from the intracellular and extracellular metabolic profiling of WT and *cia5* mutant, we confirmed the substantial accumulation of glycolate by the *cia5* mutant. Glycolate is the simplest α -hydroxy acid and is used as an exfoliant or buffering agent by improving skin texture in cosmetics and personal care products (Rendon et al., 2008). Chemists also use glycolate to synthesize polymers with excellent gas barrier properties by using glycolate alone or with other acid units, including L-lactate (Fredenberg et al., 2011). Thus, we tried to

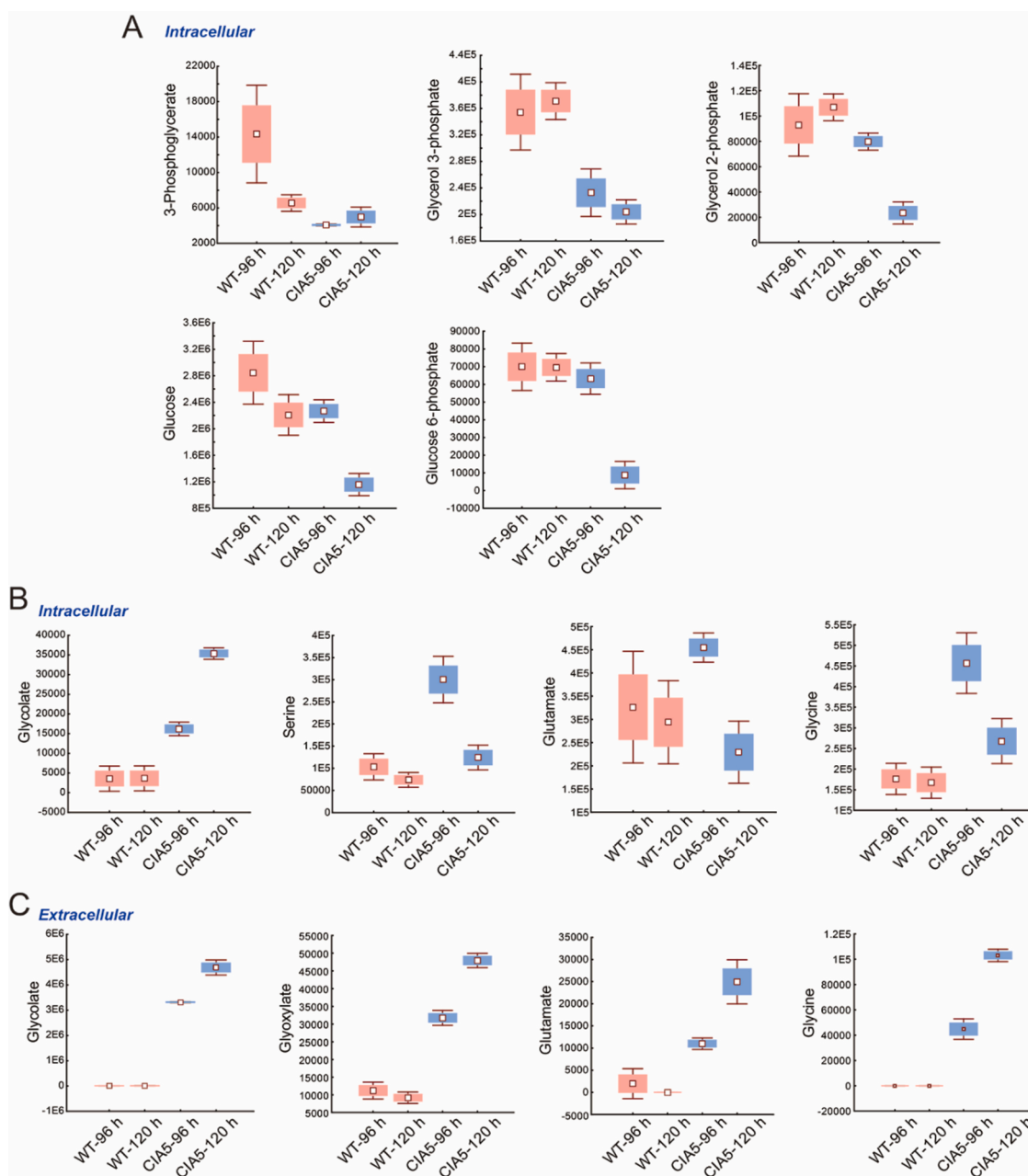


Fig. 5. The normalized abundance levels of (A) the intracellular metabolites of *Chlamydomonas reinhardtii* WT (WT) and *cia5* mutant (CIA5) strains related to (photosynthesis and glycolysis during the photoautotrophic phase (i.e., 96 h and 120 h) are shown in the box-whisker plots. The normalized abundance levels of (B) the intracellular and (C) extracellular metabolites of *Chlamydomonas reinhardtii* WT (WT) and *cia5* mutant (CIA5) strains related to photorespiration pathway during the photoautotrophic phase (i.e., 96 h and 120 h) are shown in the box-whisker plots. All experiments were performed in triplicate.

cultivate the *cia5* mutant to produce glycolate. During the photoautotrophic growth, only the *cia5* mutant produced glycolate, whereas WT did not produce glycolate (Fig. 6). After 140 h, the *cia5* mutant produced 0.3 g/L of glycolate (Fig. 6).

4. Discussion

The *CIA5* gene influences CCM function (Fang et al., 2012; Giordano et al., 2005; Xiang et al., 2001), however, there are limited descriptions of the phenotypic changes in response to the mutation of the *CIA5* gene in *C. reinhardtii*. In this study, we observed the phenotypic changes by a *cia5* mutant leading to accumulation of C2 compounds (i.e., glycolate and glyoxylate) using global metabolic profiling of intracellular and extracellular metabolites of the *cia5* mutant and WT.

During the mixotrophic phase, global metabolic profiling obtained from the intracellular and extracellular metabolites of *C. reinhardtii* WT and *cia5* mutant were similar (Fig. 3A and B). This implies that the *CIA5* gene mutation, which caused the malfunction of CCM, did not significantly change the metabolic phenotype during the mixotrophic growth phase. The similar metabolic profiles between WT and *cia5* mutant are probably due to the inhibition of photosynthesis in the presence of acetate (Heifetz et al., 2000). The genes related to CCM, including *CIA5*, are downregulated during the mixotrophic phase based on the presence of an organic carbon source (e.g., acetic acid) (Heifetz et al., 2000).

However, when the cells depleted their organic carbon supply at the onset of the photoautotrophic phase, the metabolite profiles of *C. reinhardtii* WT and *cia5* mutant were significantly changed (Fig. 3A and B). In the photoautotrophic phase, green algae *Chlamydomonas*

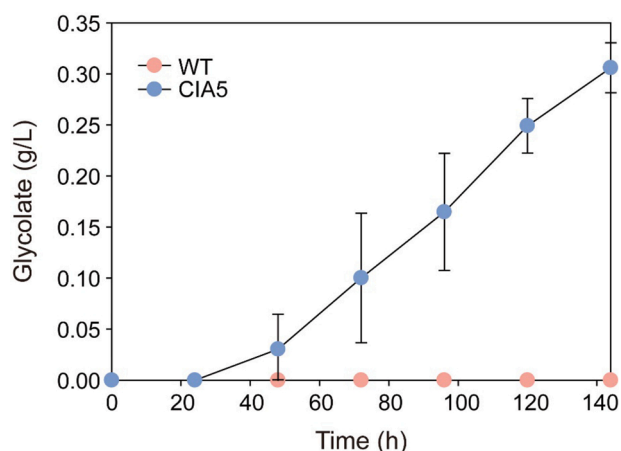


Fig. 6. Comparison of the production of glycolate by *Chlamydomonas reinhardtii* WT (WT) and *cia5* mutant (CIA5) strains. The cells of WT and CIA5 strains were cultured in liquid Tris-Acetate-Phosphate (TAP) medium on a shaker platform set at 100 rpm. The cultures were conducted in a 25 °C warm room under fluorescent light with an intensity of 65 $\mu\text{mol m}^{-2} \text{s}^{-1}$. The cultures were maintained using ambient air within the flask, and the flasks were covered with aluminum foil. There was no additional CO_2 provided. All experiments were performed in triplicate.

species synthesize organic carbon through photosynthesis (Hanikenne, 2003). The *CIA5* gene, a CCM transcriptional regulator, plays a crucial role for CCM regulation to increase CO_2 availability to Rubisco (Fang et al., 2012; Xiang et al., 2001). Based on the multivariate statistical analyses using PCA and HCA, we observed the primary metabolite profiles changes in the intermediates associated with photorespiration. The primary function of the photorespiration pathway is to generate a C3 compound (e.g., 3-phosphoglycerate) from a C2 compound (e.g., phosphoglycolate) (Dellero et al., 2016) and the concomitant evolution of a CO_2 molecule.

After acetate depletion, cells entered to photoautotrophic phase to generate the energy via photosynthesis or photorespiration. In the cells of *cia5* mutant at 120 h, abundances of the metabolites, 3-phosphoglycerate, glycerol phosphates, glucose, and glucose 6-phosphate, were significantly reduced (Fig. 5A). The insufficient metabolic activity of photosynthesis of *cia5* mutant caused by malfunction of CCM might result in a lower level of 3-phosphoglycerate (Fig. 5A). Also, glucose and glucose 6-phosphate levels are probably related to 3-phosphoglycerate levels (Fig. 5A) because C6 compounds can be synthesized from two molecules of C3 compounds. Glycerol 3-phosphate, a metabolic intermediate of the glycerolipid pathway, is crucial to provide tolerance against environmental stress such as nutrient starvation (Driver et al., 2017). The lower level of glycerol 3-phosphate in the cells of *cia5* mutant is presumed to be related to less tolerance against nutrient starvation conditions than WT (Fig. 5A).

In this study, we found that the *cia5* mutant produces substantial amounts of glycolate during the photoautotrophic growth phase with a portion of it released extracellularly. This means that although green algae *Chlamydomonas* species have a photorespiration pathway to generate C3 compounds for feeding the central metabolic pathway such as glycolysis, that there is leakage of glycolate from the photorespiratory pathway making it more energetically inefficient than it already is. Therefore, to improve the photorespiration pathway efficiency in green algae *Chlamydomonas* species, the introduction of a highly active alternative glycolate metabolism pathway is feasible (South et al., 2019). On the other hand, since the cosmetic industry uses glycolate as an ingredient, the *cia5* mutant strain has a potential role as a glycolate production factory driven by light energy.

In conclusion, we discovered that the production of glycolate by *cia5* mutant is substantial, and it offers a resource for production of this high-

value cosmetic ingredient. The metabolite profiling results revealed the accumulation of C2 compounds, including glycolate and glyoxylate, and we presume production was a consequence of an inefficient photosynthetic mechanism caused by a dysfunctional CCM in the *cia5* mutant and the inefficient photorespiration pathway requiring multiple reactions and energy. This study provides useful information to explain the effects of mutating CCM-related genes on the metabolic phenotype of photosynthetic organisms such as green algae and plants. Therefore, we demonstrated use of a metabolomic approach to understand, modify, or enhance the photosynthetic mechanisms.

CRedit authorship contribution statement

Eun Ju Yun: Conceptualization, Data curation, Investigation, Methodology, Software, Visualization, Writing - original draft. **Guo-Chang Zhang:** Formal analysis, Investigation, Methodology, Writing - original draft. **Christine Atkinson:** Data curation, Methodology, Writing - original draft. **Stephan Lane:** Validation, Writing - review & editing. **Jing-Jing Liu:** Resources, Writing - review & editing. **Donald R. Ort:** Conceptualization, Project administration, Supervision, Writing - review & editing. **Yong-Su Jin:** Conceptualization, Project administration, Supervision, Funding acquisition, Writing - review & editing.

Declaration of Competing Interest

The authors report no declarations of interest.

Acknowledgments

This work is supported by the research project Realizing Increased Photosynthetic Efficiency (RIPE) that is funded by the Bill & Melinda Gates Foundation, Foundation for Food and Agriculture Research, and the Department for International Development under grant no. OPP1172157.

Appendix A. Supplementary data

Supplementary material related to this article can be found, in the online version, at doi:<https://doi.org/10.1016/j.jbiotec.2021.06.009>.

References

- Badger, M., Kaplan, A., Berry, J., 1980. Internal inorganic carbon pool of *Chlamydomonas reinhardtii*. Evidence for a carbon dioxide-concentrating mechanism. *Plant Physiol.* 66, 407–413. <https://doi.org/10.1104/pp.66.3.407>.
- Blaby, I.K., Blaby-Haas, C.E., Tourasse, N., Hom, E.F.Y., Lopez, D., Aksoy, M., Grossman, A., Umen, J., Dutcher, S., Porter, M., King, S., Witman, G.B., Stanke, M., Harris, E.H., Goodstein, D., Grimwood, J., Schmutz, J., Vallon, O., Merchant, S.S., Prochnik, S., 2014. The *Chlamydomonas* genome project: a decade on. *Trends Plant Sci.* 19, 672–680. <https://doi.org/10.1016/j.tplants.2014.05.008>.
- Dellero, Y., Jossier, M., Schmitz, J., Maurino, V.G., Hodges, M., 2016. Photorespiratory glycolate-glyoxylate metabolism. *J. Exp. Bot.* 67, 3041–3052. <https://doi.org/10.1093/jxb/erw090>.
- Driver, T., Trivedi, D.K., McIntosh, O.A., Dean, A.P., Goodacre, R., Pittman, J.K., 2017. Two glycerol-3-phosphate dehydrogenases from *Chlamydomonas* have distinct roles in lipid metabolism. *Plant Physiol.* 174, 2083–2097.
- Fang, W., Si, Y., Douglass, S., Casero, D., Merchant, S.S., Pellegrini, M., Ladunga, I., Liu, P., Spalding, M.H., 2012. Transcriptome-wide changes in *Chlamydomonas reinhardtii* gene expression regulated by carbon dioxide and the CO_2 -concentrating mechanism regulator *CIA5/CCM1*. *Plant Cell* 24, 1876–1893. <https://doi.org/10.1105/tpc.112.097949>.
- Fredenberg, S., Wahlgren, M., Reslow, M., Axelsson, A., 2011. The mechanisms of drug release in poly(lactic-co-glycolic acid)-based drug delivery systems—a review. *Int. J. Pharm.* 415, 34–52. <https://doi.org/10.1016/j.ijpharm.2011.05.049>.
- Fukuzawa, H., Miura, K., Ishizaki, K., Kucho, K., Saito, T., Kohinata, T., Ohyama, K., 2001. *Ccm1*, a regulatory gene controlling the induction of a carbon-concentrating mechanism in *Chlamydomonas reinhardtii* by sensing CO_2 availability. *Proc. Natl. Acad. Sci. U.S.A.* 98, 5347–5352. <https://doi.org/10.1073/pnas.081593498>.
- Giordano, M., Beardall, J., Raven, J.A., 2005. CO_2 concentrating mechanisms in algae: mechanisms, environmental modulation, and evolution. *Annu. Rev. Plant Biol.* 56, 99–131. <https://doi.org/10.1146/annurev.arplant.56.032604.144052>.

- Gorman, D.S., Levine, R.P., 1965. Cytochrome f and plastocyanin: their sequence in the photosynthetic electron transport chain of *Chlamydomonas reinhardtii*. Proc. Natl. Acad. Sci. U.S.A. 54, 1665–1669. <https://doi.org/10.1073/pnas.54.6.1665>.
- Hanikenne, M., 2003. *Chlamydomonas reinhardtii* as a eukaryotic photosynthetic model for studies of heavy metal homeostasis and tolerance. New Phytol. 159, 331–340. <https://doi.org/10.1046/j.1469-8137.2003.00788.x>.
- Heifetz, P.B., Förster, B., Osmond, C.B., Giles, L.J., Boynton, J.E., 2000. Effects of acetate on facultative autotrophy in *Chlamydomonas reinhardtii* assessed by photosynthetic measurements and stable isotope analyses. Plant Physiol. 122, 1439–1445. <https://doi.org/10.1104/pp.122.4.1439>.
- Howe, E., Holton, K., Nair, S., Schlauch, D., Sinha, R., Quackenbush, J., 2010. MeV: MultiExperiment viewer. In: Ochs, M.F., Casagrande, J.T., Davuluri, R.V. (Eds.), Biomedical Informatics for Cancer Research. Springer US, pp. 267–277. https://doi.org/10.1007/978-1-4419-5714-6_15.
- Kim, S., Lee, D.Y., Wohlgemuth, G., Park, H.S., Fiehn, O., Kim, K.H., 2013. Evaluation and optimization of metabolome sample preparation methods for *Saccharomyces cerevisiae*. Anal. Chem. 85, 2169–2176. <https://doi.org/10.1021/ac302881e>.
- Kropat, J., Hong-Hermesdorf, A., Casero, D., Ent, P., Castruita, M., Pellegrini, M., Merchant, S.S., Malasarn, D., 2011. A revised mineral nutrient supplement increases biomass and growth rate in *Chlamydomonas reinhardtii*. Plant J. 66, 770–780. <https://doi.org/10.1111/j.1365-3113.2011.04537.x>.
- Kroth, P., Chiovitti, A., Gruber, A., Martin-Jezequel, V., Mock, T., Parker, M., Stanley, M., Kaplan, A., Caron, L., Weber, T., Maheswari, U., Armbrust, E., Bowler, C., 2008. A model for carbohydrate metabolism in the diatom *Phaeodactylum tricorutum* deduced from comparative whole genome analysis. PLoS One 3, e1426. <https://doi.org/10.1371/journal.pone.0001426>.
- Lee, D.Y., Fiehn, O., 2008. High quality metabolomic data for *Chlamydomonas reinhardtii*. Plant Methods 4, 7. <https://doi.org/10.1186/1746-4811-4-7>.
- Marek, L.F., Spalding, M.H., 1991. Changes in photorespiratory enzyme activity in response to limiting CO₂ in *Chlamydomonas reinhardtii*. Plant Physiol. 97, 420. <https://doi.org/10.1104/pp.97.1.420>.
- Merchant, S.S., Prochnik, S.E., Vallon, O., Harris, E.H., Karpowicz, S.J., Witman, G.B., Terry, A., Salamov, A., Fritz-Laylin, L.K., Maréchal-Drouard, L., Marshall, W.F., Qu, L.-H., Nelson, D.R., Sanderfoot, A.A., Spalding, M.H., Kapitonov, V.V., Ren, Q., Ferris, P., Lindquist, E., Shapiro, H., Lucas, S.M., Grimwood, J., Schmutz, J., Cardol, P., Cerutti, H., Chanfreau, G., Chen, C.-L., Cognat, V., Croft, M.T., Dent, R., Dutcher, S., Fernández, E., Fukuzawa, H., González-Ballester, D., González-Halphen, D., Hallmann, A., Hanikenne, M., Hippler, M., Inwood, W., Jabbari, K., Kalanon, M., Kuras, R., Lefebvre, P.A., Lemaire, S.D., Lobanov, A.V., Lohr, M., Manuell, A., Meier, I., Mets, L., Mittag, M., Mittelman, T., Moroney, J.V., Moseley, J., Napoli, C., Nedelcu, A.M., Niyogi, K., Novoselov, S.V., Paulsen, I.T., Pazour, G., Purton, S., Ral, J.-P., Riaño-Pachón, D.M., Riekhof, W., Rymarquis, L., Schroda, M., Stern, D., Umen, J., Willows, R., Wilson, N., Zimmer, S.L., Allmer, J., Balk, J., Bisova, K., Chen, C.-J., Elias, M., Gendler, K., Hauser, C., Lamb, M.R., Ledford, H., Long, J.C., Minagawa, J., Page, M.D., Pan, J., Pootakham, W., Roje, S., Rose, A., Stahlberg, E., Terauchi, A.M., Yang, P., Ball, S., Bowler, C., Dieckmann, C. L., Gladyshev, V.N., Green, P., Jorgensen, R., Mayfield, S., Mueller-Roeber, B., Rajamani, S., Sayre, R.T., Brokstein, P., Dubchak, I., Goodstein, D., Hornick, L., Huang, Y.W., Jhaveri, J., Luo, Y., Martínez, D., Ngau, W.C.A., Otilar, B., Poliakov, A., Porter, A., Szajkowski, L., Werner, G., Zhou, K., Grigoriev, I.V., Rokhsar, D.S., Grossman, A.R., 2007. The *Chlamydomonas* genome reveals the evolution of key animal and plant functions. Science 318, 245–250. <https://doi.org/10.1126/science.1143609>.
- Moroney, J.V., Husic, H.D., Tolbert, N.E., Kitayama, M., Manuel, L.J., Togaaki, R.K., 1989. Isolation and characterization of a mutant of *Chlamydomonas reinhardtii* deficient in the CO₂ concentrating mechanism. Plant Physiol. 89, 897–903. <https://doi.org/10.1104/pp.89.3.897>.
- Rendon, M., Cardona, L.M., Bussear, E.W., Benitez, A.L., Colón, L.E., Johnson, L.A., 2008. Successful treatment of moderate to severe melasma with triple-combination cream and glycolic acid peels: a pilot study. Cutis 82, 372–378.
- Riekhof, W.R., Sears, B.B., Benning, C., 2005. Annotation of genes involved in glycerolipid biosynthesis in *Chlamydomonas reinhardtii*: discovery of the betaine lipid synthase BTA1_{CR}. Eukaryot. Cell 4, 242. <https://doi.org/10.1128/EC.4.2.242-252.2005>.
- Rochaix, J.-D., 2002. *Chlamydomonas*, a model system for studying the assembly and dynamics of photosynthetic complexes. FEBS Lett. 529, 34–38. [https://doi.org/10.1016/S0014-5793\(02\)03181-2](https://doi.org/10.1016/S0014-5793(02)03181-2).
- South, P.F., Cavanagh, A.P., Liu, H.W., Ort, D.R., 2019. Synthetic glycolate metabolism pathways stimulate crop growth and productivity in the field. Science 363, eaat9077. <https://doi.org/10.1126/science.aat9077>.
- Stein, S.E., 1999. An integrated method for spectrum extraction and compound identification from gas chromatography/mass spectrometry data. J. Am. Soc. Mass Spectrom. 10, 770–781. [https://doi.org/10.1016/S1044-0305\(99\)00047-1](https://doi.org/10.1016/S1044-0305(99)00047-1).
- Styczynski, M.P., Moxley, J.F., Tong, L.V., Walther, J.L., Jensen, K.L., Stephanopoulos, G. N., 2007. Systematic identification of conserved metabolites in GC/MS data for metabolomics and biomarker discovery. Anal. Chem. 79, 966–973. <https://doi.org/10.1021/ac0614846>.
- Xiang, Y., Zhang, J., Weeks, D.P., 2001. The *Cia5* gene controls formation of the carbon concentrating mechanism in *Chlamydomonas reinhardtii*. Proc. Natl. Acad. Sci. U.S.A. 98, 5341–5346. <https://doi.org/10.1073/pnas.101534498>.